



Polyoxometalate-based manganese clusters as catalysts for efficient photocatalytic and electrochemical water oxidation



Li Yu^a, Yong Ding^{a,b,*}, Min Zheng^a

^a State Key Laboratory of Applied Organic Chemistry, Key Laboratory of Nonferrous Metals Chemistry and Resources Utilization of Gansu Province, and College of Chemistry and Chemical Engineering, Lanzhou University, Lanzhou 730000, China

^b State Key Laboratory for Oxo Synthesis and Selective Oxidation, Lanzhou Institute of Chemical Physics, Chinese Academy of Sciences, Lanzhou 730000, China

ARTICLE INFO

Article history:

Received 4 November 2016

Received in revised form 10 January 2017

Accepted 18 February 2017

Available online 21 February 2017

Keywords:

Polyoxometalate

Photocatalytic water oxidation

Electrochemical water oxidation

Homogeneous molecular catalyst

ABSTRACT

A manganese containing polyoxometalate (POM) $[\text{Mn}_3(\text{H}_2\text{O})_3(\text{SbW}_9\text{O}_{33})_2]^{12-}$ (**1**) was synthesized and characterized in detail. The photocatalytic activity of **1** is definitely better than other manganese containing POM water oxidation catalysts reported so far according to oxygen yield, whereas the analogues $[\text{Mn}_3(\text{H}_2\text{O})_5(\text{PW}_9\text{O}_{34})_2]^{12-}$ (**2**) and $[\text{Mn}_3(\text{H}_2\text{O})_3(\text{AsW}_9\text{O}_{33})_2]^{12-}$ (**3**) show no to slight photocatalytic O_2 evolution amount. Meanwhile, the electrocatalytic activities of **1–3** were investigated in 80 mM pH 9.0 borate buffer, which follows the catalytic activity order of **1** > **2** > **3**. Multiple experiments including UV–vis absorption, catalysts aging experiments, tetra-*n*-heptylammonium nitrate (THpANO₃) toluene extraction, electrochemical experiments and capillary electrophoretic measurements results confirm that catalyst **1** is a homogeneous molecular catalyst. No Mn²⁺ (aq.) or manganese oxide under the reaction conditions of photocatalytic and electrochemical water oxidation was detected.

© 2017 Elsevier B.V. All rights reserved.

1. Introduction

Energy is a universal human requirement and most energy is derived from fossil fuels. Some of which are rapidly exhausting, and their final product is CO₂, a major source of anthropogenic global warming. To address those issues, we should exploit more renewable and carbon-neutral energy sources of sufficient scale [1–4]. Splitting water into H₂ and O₂ by sunlight is considered as one of the most promising ways to produce green and renewable energy, which is expected to meet the rising global energy demand in future. Photolysis of water consists of two half-reactions: the reduction of protons to H₂ and the oxidation of water to O₂ [5]. The oxidation of water can be viewed as a vital step of the energy-transfer process in both natural and artificial photosynthesis [6]. Therefore, the development of stable, efficient, and low-cost water oxidation catalysts (WOCs) has become especially important for the conversion of sunlight into green and accumulation chemical energy [7]. Just in the last few years, under photochemical or elec-

trochemical conditions, a lot of meaningful WOCs based on Cu [8,9], Ni [10,11], Fe [12,13], Co [14,15], and Mn [16,17] elements have been developed for water oxidation. Among the various transition-metal-based WOCs, manganese is a very abundant element in the Earth's crust and Mn-based compounds are already considered to be one of prominent WOCs due to their characteristic of non-toxic and excellent water oxidation ability. What is more, Mn-based compounds containing cubane unit can function as models for the catalytic Mn₄CaO₅ center in the oxygen evolving complex (OEC) of photosystem II (PSII) [18].

In the last couple of years, there were various kinds of WOCs have been developed for water oxidation. One of the most promising WOCs is polyoxometalates (POMs) because they can stand against fast, invertible, and stepwise multielectron-transfer reactions without changing their structures [19–22]. It should be noted that the introduction of transition metal into POMs can adjust the band gap structures and even broaden the absorption range from UV to visible light region of such molecular clusters [23,24]. Recently, a mass of POMs based on Cu [25], Ni [26–28], Fe [29], Co [30–37], Mn [16,38], and V [39] have been researched extensively as catalysts for water oxidation by different groups. However, in contrast to other transition metal-based WOCs, few manganese containing POM as WOCs have been achieved for water oxidation.

Herein, we first report manganese containing POM of $[\text{Mn}_3(\text{H}_2\text{O})_3(\text{SbW}_9\text{O}_{33})_2]^{12-}$ (**1**) as an efficient photocatalytic and

* Corresponding author at: State Key Laboratory of Applied Organic Chemistry, Key Laboratory of Nonferrous Metals Chemistry and Resources Utilization of Gansu Province, and College of Chemistry and Chemical Engineering, Lanzhou University, Lanzhou, 730000, China.

E-mail addresses: dingyong1@lzu.edu.cn, dingyong1973@163.com (Y. Ding).

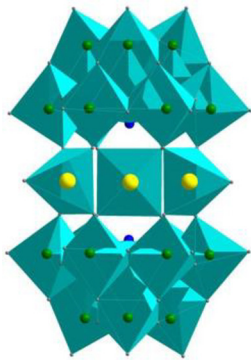
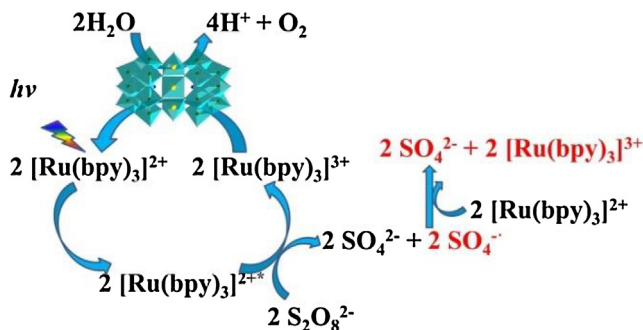


Fig. 1. Combined polyhedral representation of **1**. The color code is as follows: manganese, yellow; tungsten, green; antimony, blue; oxygen, gray.



Scheme 1. Principal processes of an O_2 evolution light-driven water oxidation system.

electrochemical water oxidation catalyst. This Mn-substituted POM **1** was first reported by Bernt Krebs and co-workers in 1998 [40]. The heteropolyanion **1** consists of two identical $Na_9[SbW_9O_{33}]$ Keggin portion, in which the arrangement of the WO_6 octahedron around the SbO_3 pyramid. The two Keggin portion are linked together by three manganese (II) ions, leading to a sandwich-type assembly (Fig. 1). **1** was made up of only earth-abundant elements (manganese, antimony, tungsten, and oxygen), which can catalyze water oxidation under photochemical and electrochemical conditions. The catalytic ability of **1** was compared with its analogues: $[Mn_3(H_2O)_5(PW_9O_{34})_2]^{9-}$ (**2**) and $[Mn_3(H_2O)_3(AsW_9O_{33})_2]^{12-}$ (**3**) and other POMs containing Mn with different structures. Furthermore, the corresponding simple manganese salt ($MnCl_2 \cdot 4H_2O$) was investigated as control comparison experiment for water oxidation. Under reaction conditions, a turn-over number (TON) of 103 and turn-over frequency (TOF_{initial}) of 0.4 s^{-1} over **1** were obtained for the photocatalytic water oxidation and the analogues **2** and **3** show no to slight activity. The same reactive activity sequence is further supported by electrocatalytic behavior. The reaction mechanism of the visible light-driven water oxidation catalyzed by **1** is depicted in Scheme 1.

2. Experiment section

2.1. Materials

All chemicals and salts (analytical grade) were used as received without any further purification. $Na_9[SbW_9O_{33}]$, $Na_9[A-a-PW_9O_{34}]$ and $Na_9[\alpha-AsW_9O_{33}]$ were synthesized according to the literature [41,42]. Purified water ($18.2\text{ M}\Omega\text{ cm}$) for the preparation of solutions was attained from a Molecular Lab Water Purifier.

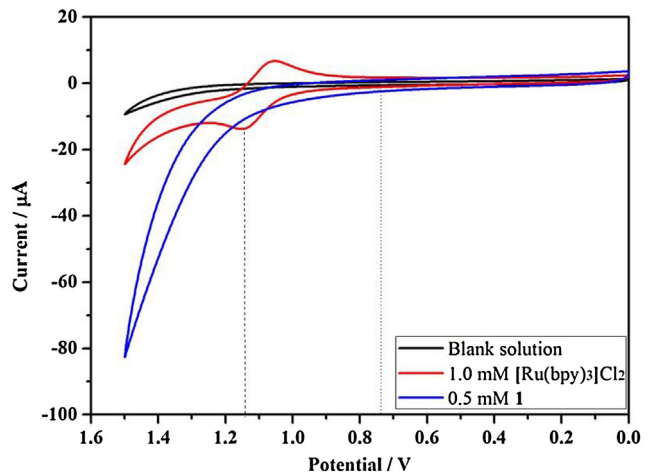


Fig. 2. CV of 0.5 mM **1** (blue curve) and 1.0 mM $[Ru(bpy)_3]Cl_2$ (red curve) in borate buffer solution (80 mM, pH 9.0). Black curve shows the CV curve of borate buffer (80 mM, pH 9.0) in the absence of **1** and $[Ru(bpy)_3]Cl_2$. Conditions: glassy carbon working electrode, Ag/AgCl (saturated KCl) reference electrode and Pt wire counter electrode; scan rate 100 mV/s. (For interpretation of the references to colour in this figure legend, the reader is referred to the web version of this article.)

2.2. Catalyst preparation

$Na_{11}(NH_4)[(Mn(H_2O))_3(SbW_9O_{33})_2]$ ($Na_{11}(NH_4)$ -**1**). $Na_{11}(NH_4)$ -**1** was synthesized according to the report by Bernt Krebs [40]. 4 g of $Na_9[SbW_9O_{33}]$ was dissolved in 8 mL water with gentle heating. 0.414 g of $MnCl_2 \cdot 4H_2O$ in 10 mL water was then added slowly to the above system with stirring and resulting in an orange solution with pH 6–7. This solution was refluxed for 1 h, and then 0.673 g of NH_4NO_3 was added, allowed to cool. Slow evaporation of the mixture at ambient temperature led to the formation of dark orange crystals of $Na_{11}(NH_4)$ -**1** within several days. Yield: 35 mg. FT-IR (cm^{-1}) for $Na_{11}(NH_4)$ -**1**: 938, 835, 770, 717. Elemental analysis calculated (%) for **1**: Mn, 2.78. Found: Mn, 2.89.

$K_6Cs[C(NH_2)_3]_2[Mn_3(H_2O)_5(PW_9O_{34})_2]$ ($K_6Cs[C(NH_2)_3]_2$ -**2**). $K_6Cs[C(NH_2)_3]_2$ -**2** was synthesized according to a procedure reported by Ulrich Kortz [43]. Yield: 29 mg. FT-IR (cm^{-1}) for $K_6Cs[C(NH_2)_3]_2$ -**2**: 1085, 1027, 945, 900, 790, 596. Elemental analysis calculated (%) for **2**: Mn, 2.93. Found: Mn, 3.05.

$K_{11}Na_1[Mn_3(H_2O)_3(AsW_9O_{33})_2]$ ($K_{11}Na_1$ -**3**). $K_{11}Na_1$ -**3** was synthesized according to a procedure reported by Pierre Mialane [44]. Yield: 58 mg. FT-IR (cm^{-1}) for $K_{11}Na_1$ -**3**: 1087, 1046, 1013, 933, 876, 829, 773, 598, 520. Elemental analysis calculated (%) for **3**: Mn, 2.90. Found: Mn, 3.08.

3. Results and discussion

3.1. Photocatalytic water oxidation performance

In order to investigate the ability of **1** catalyzing water oxidation, the cyclic voltammetry (CV) characterizations was performed with $[Ru(bpy)_3]Cl_2$ and **1**. As shown in Fig. 2, a catalytic water oxidation wave of **1** is observed at onset potential at approximately 0.72 V (vs. Ag/AgCl). However, in the absence of **1**, no obvious catalytic current was detected in the same reaction conditions and operation procedure. So it is demonstrable that **1** has the ability to catalyze the water-oxidation reaction. In addition, the redox potential of $[Ru(bpy)_3]^{3+}/[Ru(bpy)_3]^{2+}$ in the same reaction system is much more positive (1.14 V vs Ag/AgCl) than the onset potential of the catalyst (Fig. 2 dash curve and dot curve). Considering the

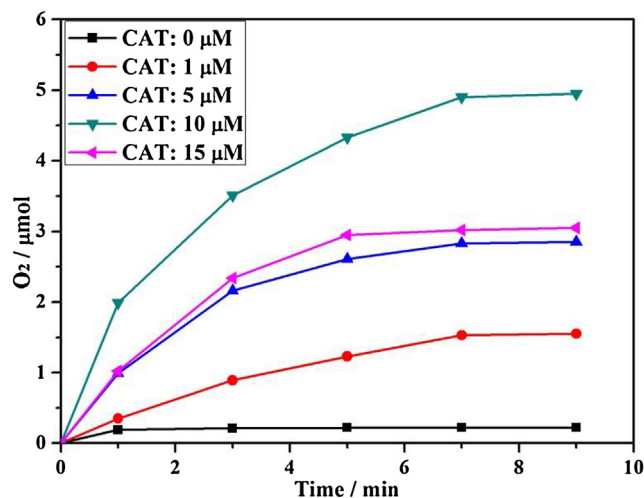


Fig. 3. Kinetics of O_2 formation in the photocatalytic system using different concentrations of **1**. Conditions: LED lamp ($\lambda \geq 420$ nm), 1.0 mM $[Ru(bpy)_3]Cl_2$, 5.0 mM $Na_2S_2O_8$, 80 mM sodium borate buffer (initial pH 9.0), total reaction volume is 15 mL.

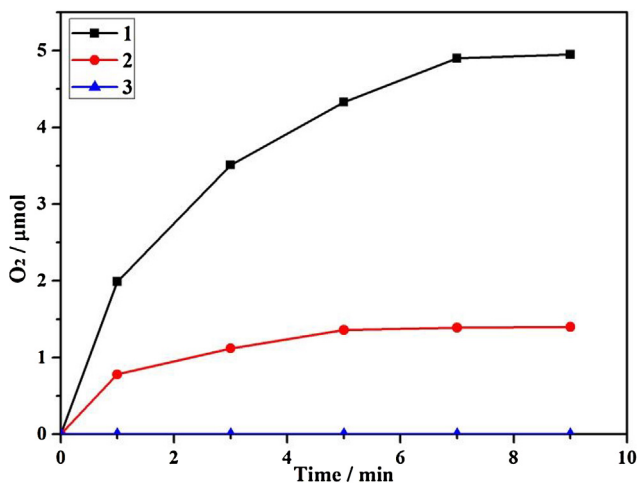


Fig. 4. Kinetics of O_2 formation in the photocatalytic system using **1** (black), **2** (red) and **3** (blue). Conditions: LED lamp ($\lambda \geq 420$ nm), 1.0 mM $[Ru(bpy)_3]Cl_2$, 5.0 mM $Na_2S_2O_8$, 10 μ M **1–3**, 80 mM sodium borate buffer (initial pH 9.0), total reaction volume is 15 mL. (For interpretation of the references to colour in this figure legend, the reader is referred to the web version of this article.)

above facts, the process of water oxidation driven by photogenerated $[Ru(bpy)_3]^{3+}$ is thermodynamically capable.

The photocatalytic water oxidation abilities of **1–3** were investigated in the $[Ru(bpy)_3]Cl_2$ ($bpy = 2,2'$ -bipyridine)/visible-light illumination/ $Na_2S_2O_8$ reaction system ($[Ru(bpy)_3]^{2+} - S_2O_8^{2-} - light$). In this system, $[Ru(bpy)_3]Cl_2$ was used as a photosensitizer, $S_2O_8^{2-}$ as a sacrificial electron acceptor and **1–3** as the catalysts for oxygen evolution in sodium borate buffer. The experimental system was carried out at different catalyst concentrations (0–15 μ M) with 15 mL of reaction solution, and their photocatalytic performances are shown in Figs. 3–4 and Table S1–S2. As demonstrated in Fig. 3, the O_2 was generated quickly after 1 min of visible light illumination, while O_2 evolution rate starts decline over time and keeps at a steady platform in 9 min. A maximum O_2 yield (13.2% for **1**, 3.9% for **2**, and 0% for **3**) and an O_2 evolution amount (4.95 μ mol for **1**, 1.46 μ mol for **2**, and 0 μ mol for **3**) were obtained for **1–3** at the optimum conditions (Table S1–S2). The catalytic activity of **1** increased with an increase within the concentration of **1** up to 10 μ M. But when the concentration of **1** rose above 10 μ M, the O_2 yield

decreased, showing a saturation-inhibition behavior for **1** > 10 μ M. The reaction system became turbid during photocatalytic water oxidation process when the concentration of **1** was increased above 10 μ M. An insoluble substance appeared in the reaction solution, whereas this phenomenon was not observed when lower catalyst concentrations were performed (≤ 10 μ M). The proposed reason for this phenomenon is that a large cationic dye-POM conjugate was formed when the high catalyst concentrations of **1** (> 10 μ M) was used. The appearance of conjugate is negative for water oxidation activity. The O_2 evolution amount corresponds to a high TON of 103 for **1**, 27 for **2**, and 0 for **3**, respectively. Therefore, the photocatalytic water oxidation abilities of **1–3** follow the order of **1** > **2** > **3** (Fig. 4, Table S1–S2 and Fig. S12). For **1–3**, they have analogous structure and different heteroatoms (Sb-centered, P-centered and As-centered POMs, respectively). The comparison of the catalytic activity among **1–3** for water oxidation provides a rule about the influence of heteroatoms on oxygen evolution: Sb > P > As. Therefore, we can draw a conclusion that different kinds of heteroatoms in the polyoxoanion affect the photocatalytic water oxidation activity.

Moreover, under the optimum reaction conditions, the control experiments were performed (Fig. S13). Only 0.22 μ mol O_2 was detected after 9 min irradiation in the absence of **1**, which came from the background oxidation of water by $[Ru(bpy)_3]^{3+}$ generated by light irradiation in the presence of $Na_2S_2O_8$. It is concluded that catalyst **1** is catalytically active and can promote the O_2 evolution during the photocatalytic water oxidation process. As shown in Fig. S13, there was no detectable O_2 in the presence of **1** without $[Ru(bpy)_3]Cl_2$, $Na_2S_2O_8$ or light, revealing photosensitizer, sacrificial electron acceptor and light are indispensable to photocatalytic water oxidation. In the meantime, other three reaction conditions including buffer pH values, photosensitizer concentrations and oxidant concentrations of water oxidation were optimized to obtain the optimum reaction conditions (Fig. S14–S16).

Other six manganese-substituted POMs as the catalysts for light-driven water oxidation were further investigated at the optimum reaction conditions for comparison (Table 1), such as $[Mn_3(OH)_3(H_2O)_3(A-\alpha-SiW_9O_{34})]^{7-}$, $[Mn_2SiW_{10}O_{37}(OH)(H_2O)]^{6-}$, $[(MnSiW_{11}O_{38}OH)_3]^{15-}$, $[Mn_4(CH_3COO)_3(A-\alpha-SiW_9O_{34})]^{6-}$ (Mn_4) and so on. Among these POMs, only Mn_4 POM gave a moderate O_2 yield of 5.6%, while none of others show any O_2 evolution. Therfore, the activities of the catalysts correlate with the specific structure of POMs rather than the number of manganese. The specific structure of **1** endows it a superior catalytic water oxidation performance.

3.2. Reuse of the catalyst

The reuse experiment of catalyst was performed as follows: after the first run, 17.8 mg (5 mM) of $Na_2S_2O_8$ was then added to the reaction solution. In the second run, only 3 μ mol O_2 was detected after 9 min irradiation under the same reaction conditions and operation as the first run. Compared with the first run, the O_2 yield of the second one reduced from 13.2% to 8.0% and the corresponding TON reduced from 33 to 20 (Fig. S17). At the end of the first run and the second run, two obvious phenomena were found in this experimental system: (1) the color of reaction solution became deeper (photosensitizer is decomposed); (2) the pH values after the first run and the second run decreased from 9.0 to 8.35 and 8.01, respectively. There are two reasons that account for the decrease of O_2 evolution during the recycle experiment: (1) the concentration of photosensitizer becomes small; (2) the pH of reaction solution is decreased, i.e., a low pH value is bad for water oxidation (Fig. S14). Besides, another recycle experiment of photocatalytic water oxidation was carried out as follows: In order to regulate the concentration of photosensitizer and the pH value of the reaction

Table 1Water oxidation catalyzed by different manganese-containing POMs.^a

Entry	Catalyst	O ₂ yield ^b (%)
1	[Mn ₃ (H ₂ O) ₃ (SbW ₉ O ₃₃) ₂] ¹²⁻ (1)	13.2
2	[Mn ₃ (H ₂ O) ₅ (PW ₉ O ₃₄) ₂] ⁹⁻ (2)	3.8
3	[Mn ₃ (H ₂ O) ₃ (AsW ₉ O ₃₃) ₂] ¹²⁻ (3)	0
4	[Mn ₃ (OH) ₃ (H ₂ O) ₃ (A- α -SiW ₉ O ₃₄)] ⁷⁻	0
5	[Mn ₂ SiW ₁₀ O ₃₇ (OH)(H ₂ O)] ⁶⁻	0
6	[MnSiW ₁₁ O ₃₈ OH] ₃ ¹⁵⁻	0
7	[Mn ₁₄ O ₁₂ (PO ₄) ₄ (PW ₉ O ₃₄) ₄] ³¹⁻	0
8	[Mn ₁₉ (OH) ₁₂ (SiW ₁₀ O ₃₇) ₆] ³⁴⁻	0
9	[Mn ₄ (CH ₃ COO) ₃ (A-a-SiW ₉ O ₃₄)] ⁶⁻	5.6
10 ^c	[Mn ₄ V ₄ O ₁₇ (OAc) ₃] ³⁻	7.2

^a Conditions: LED lamp ($\lambda \geq 420$ nm); 10 μ M catalyst, 1.0 mM [Ru(bpy)₃]Cl₂, 5.0 mM Na₂S₂O₈, 80 mM sodium borate buffer (initial pH 9.0), total reaction volume is 15 mL.

^b O₂ Yield = 2 \times mol of O₂ per mole of Na₂S₂O₈.

^c Conditions: LED light source ($\lambda = 470$ nm), 0.3 μ M catalyst, 1.0 mM [Ru(bpy)₃]²⁺, 10.0 mM S₂O₈²⁻, MeCN/H₂O (9:1, v/v), total reaction volume is 10 mL. Details see ref 38.

solution back to the original values of 1 mM and 9.0, 0.5 equivalent of the [Ru(bpy)₃]Cl₂ was added to the reaction system together with 17.8 mg of Na₂S₂O₈ at the end of the first run, and then the second run was performed according to the above same procedure. Nevertheless, the O₂ evolution amount was slightly higher than the blue curve in Fig. S17. The result of above experiments shows that the reaction solution environment is very complicated. After the first run of photocatalytic water oxidation, the changed environment of reaction solution affects the catalytic behavior of **1** in the recycle experiment.

3.3. Stability study

The stability of catalysts is very critical and is the central feature during photocatalytic water oxidation process. For water oxidation catalysts, there are three types of stability should be researched, i.e. oxidative, hydrolytic and thermal [45]. Because our experiment system was performed at room temperature, so it is unnecessary to consider thermal stability.

Firstly, the hydrolytical stability of **1** in aqueous solution by UV-vis spectroscopy and catalyst aging experiments were investigated. UV-vis spectra of compound **1** were recorded in pH 9.0 sodium borate buffer solution with different aging time. As shown in Fig. S18 and S19, the absorbance intensity of **1** in these UV-vis spectra remains unchanged within 3 days. The good stability of **1** (**Mn₃Sb**) is further confirmed by catalyst aging experiments. As shown in Fig. S20, compared with the aging experiment of catalyst **2** (**Mn₃P**), catalyst **1** aged 2 days has similar catalytic water oxidation activity as that of the fresh catalyst. While the oxygen yield of catalyst **2** aged 2 days has decreased to two thirds of the original value, indicating catalyst **2** is not stable. From these experimental results, we conclude that the heteroatoms in the polyoxoanion play an important role for the stability during the water oxidation process. The UV-vis analysis of catalyst **1** was carried out in pH 9.0 sodium borate buffer solution in the presence of Na₂S₂O₈ with different aging time. The absorbance intensity of **1** in this case shows the coincident curves after 2 days, indicating that the stability of **1** is not affected in an oxidizing environment (Fig. S21).

Secondly, the oxidative stability of the catalyst was studied by IR and X-ray photoelectron spectroscopy (XPS). Recycled catalyst of **1** was isolated from reaction solution after the first run by acetone precipitation method (see SI). As shown in Fig. S22, the FT-IR spectrum of recycled catalyst is almost identical to that of the fresh sample. In addition, XPS full scan measurements were conducted for the energy regions Mn 2p, Sb 3d, W 4f and O 1s, in which the binding energy of each element was corrected by a C 1s peak (284.8 eV) (Fig. S23). As depicted in Fig. S23, the XPS spectra of Mn

2p_{3/2} and Mn 2p_{1/2} peaks for the fresh catalyst **1** are located at 640.6 eV and 652.5 eV, respectively. The peaks for **1** after the reaction of Mn 2p_{3/2} and Mn 2p_{1/2} are located at 640.7 eV and 652.6 eV, respectively. The main peaks positions of Mn 2p, Sb 3d, W 4f and O 1s in **1** after water oxidation reaction are nearly the same as the fresh ones, revealing that **1** has the good stability and keeps intact after water oxidation. Based on the XPS analysis, we conclude that there are no changes in the valence states of Mn, Sb, W and O for the recovered catalyst. In the meantime, the catalytic behavior of recovered catalyst was investigated and shown similar catalytic water oxidation activity as that of the fresh catalyst (Fig. S24). The reason for slight reduction amount of O₂ evolved should be due to the loss of recovered catalyst.

Thirdly, laser flash photolysis was conducted for analysis the electron transfer between catalyst and [Ru(bpy)₃]³⁺. In photocatalytic water oxidation, the electron transfer rate from the catalyst to the oxidized photosensitizer is a key point, which can determine the overall efficiency of photoactivated cycles. A fast electron transfer rate is conducive to a high turnover frequency (TOF) for catalyst during photocatalytic water oxidation reaction. This reaction process can be expediently investigated by the experiment of laser flash photolysis, where [Ru(bpy)₃]³⁺ is generated in-situ quickly through reaction of Ru(bpy)₃²⁺ with S₂O₈²⁻ by 445 nm laser activation. The following reaction of Ru(bpy)₃³⁺ with **1** was analyzed in a ms timescale by detecting the absorption at 450 nm. The result of laser flash photolysis was obtained in 80 mM borate buffer (pH 9.0) solutions containing 50 μ M [Ru(bpy)₃]Cl₂, 5 mM Na₂S₂O₈ and 0–100 μ M **1**, which was measured at 450 nm. As shown in Fig. S25, when catalyst **1** was not added to the reaction system during photocatalytic water oxidation, the bleach persistence, i.e. constant [Ru(bpy)₃]³⁺ concentration is obtained (black line). When a certain amount of **1** was added to the reaction system, the phenomenon of quenching [Ru(bpy)₃]³⁺ is rather obvious. The above result indicated that with the increasing concentration of **1**, the hole-scavenging activity increase gradually. Therefore, the reaction system would return to the initial bleach level in the end with the concentration of **1** increasing. However, it is regretful that a large cationic dye–POM conjugate precipitate appeared in the course of the experiment when a higher catalyst concentration of **1** is used. The appearance of adduct precipitate is negative for the overall results of the flash photolysis. So the higher concentrations of **1** (>100 μ M) is not employed for laser flash photolysis experiments. Nanosecond laser flash photolysis method not only has insight into the electron transfer rate, but also investigate whether **1** is stable or not during photocatalytic water oxidation process. As shown in Fig. 5, when catalyst **1** was not added to the reaction system during reaction, the bleach persistence, i.e. constant [Ru(bpy)₃]³⁺ concentration is obtained (black line), while the other traces demonstrate the apparent reduction of [Ru(bpy)₃]³⁺ in the presence of **1**. With the increase of aging time, the hole-scavenging activity of **1** remains constant. Considering the above description, **1** has the oxidative stability over this time-scale.

Fourthly, the capillary electrophoretic method was applied to detect the stability of **1** in water oxidation system. According to charge to size ratio, the capillary electrophoretic method can separate species in the interior of a small capillary filled with an electrolyte. Therefore, this method was carried out to investigate the stability of **1** during photocatalytic water oxidation. In spite of the characteristic peaks of **1** before and after photocatalytic reactions shift slightly in the direction towards right, the peaks of **1** basically remain unchanged (Fig. 6). The reason for shift is that electrolyte concentration has changed before and after the water oxidation reactions. No extra peaks of Mn species were observed in electropherogram after water oxidation experiment. The capillary electrophoretic result demonstrates that the structure of **1** is unchanged after the water oxidation reactions.

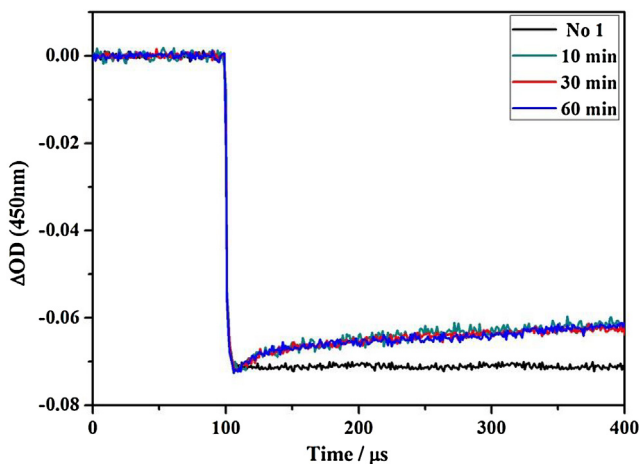


Fig. 5. Hole-scavenging kinetics measured using $10 \mu\text{M}$ of **1** at various aging times. Kinetics of bleach recovery were collected in the following experimental conditions: excitation wavelength = 445 nm; analysis wavelength = 450 nm; Containing $50 \mu\text{M}$ $[\text{Ru}(\text{bpy})_3]\text{Cl}_2$, $5.0 \text{ mM Na}_2\text{S}_2\text{O}_8$ in 80 mM sodium borate buffer ($\text{pH} = 9.0$).

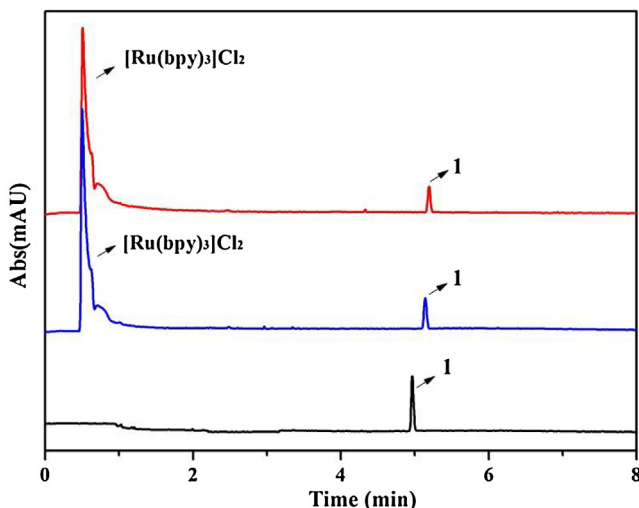


Fig. 6. An electropherogram for **1**. Black line: $10 \mu\text{M}$ of **1** in a 20 mM sodium borate buffer solution ($\text{pH} = 9.0$). Blue line: $10 \mu\text{M}$ of **1** in a 20 mM sodium borate buffer solution ($\text{pH} = 9.0$) containing $[\text{Ru}(\text{bpy})_3]\text{Cl}_2$ ($1.0 \mu\text{M}$), $\text{Na}_2\text{S}_2\text{O}_8$ (5.0 mM) before illumination. Red line: $10 \mu\text{M}$ of **1** in a 20 mM sodium borate buffer solution ($\text{pH} = 9.0$) containing $[\text{Ru}(\text{bpy})_3]\text{Cl}_2$ ($1.0 \mu\text{M}$), $\text{Na}_2\text{S}_2\text{O}_8$ (5.0 mM) after 9 min of illumination. (For interpretation of the references to colour in this figure legend, the reader is referred to the web version of this article.)

Fifthly, the extraction experiments were carried out to further investigate the stability of **1** during photocatalytic water oxidation. As a Keggin anion cluster, **1** can be separated from reaction solution with the method of tetra-*n*-heptylammonium nitrate (THpANO₃) toluene extraction, and this extraction method does not alter the original reaction system. However, MnO_x and Mn²⁺ (aq.) can not be extracted into organic layer by THpANO₃ toluene extraction method. As shown in Fig. S26, the black curve represents the kinetics of O₂ formation of **1** in the photocatalytic system under the optimum reaction conditions (O₂ yield is 13.2%). The red line represents the kinetics of O₂ formation in the photocatalytic system with extraction of **1**, followed by addition of $10 \mu\text{M}$ **1**, $[\text{Ru}(\text{bpy})_3]\text{Cl}_2$ and $\text{Na}_2\text{S}_2\text{O}_8$. From the experimental aforementioned, it can be seen that the O₂ yield (12.5%) of **1** is basically remained unchanged after extraction. After extracting **1** from reaction solutions, no obvious oxygen evolution is observed for other control experiments and the

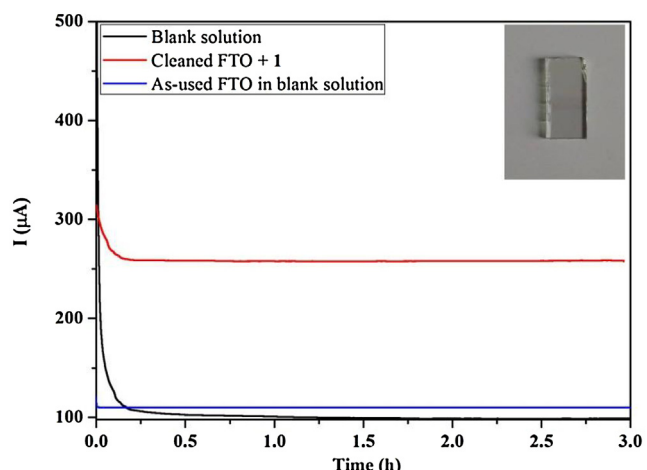


Fig. 7. Water electrolysis under an applied voltage of 1.2 V vs Ag/AgCl electrode in a $\text{pH} = 9.0$ sodium borate buffer (80 mM) solution. Initial blank (black line); 0.5 mM **1** (red line); blank after **1**-catalyzed electrolysis (blue line). Conditions: FTO glass working electrode, Ag/AgCl (saturate KCl) reference electrode and Pt wire counter electrode. Inset: The picture of FTO after electrolysis. (For interpretation of the references to colour in this figure legend, the reader is referred to the web version of this article.)

catalytic activity is similar to the blank one (Fig. S26). To prove the catalytic activity stems from **1** even further, different concentrations of MnCl₂ (1–30 μM) were investigated at the same reaction conditions. As shown in Fig. S27–S30, **1** always shows a higher catalytic activity than those of the Mn²⁺ (aq.). An induction period in the early stage of O₂ evolution catalyzed by MnCl₂ is observed during water oxidation reaction. According to the difference of catalytic activity and catalytic behavior of **1** and the Mn²⁺ (aq.), we may safely draw the conclusion that **1** is a true molecular water oxidation catalyst in this photocatalytic reaction.

3.4. Electrocatalytic water oxidation performance

The difference in the electrocatalytic activity and electrocatalytic behavior between **1** and the equivalent Mn²⁺ (aq.) were investigated through electrolysis, CV and electrochemical impedance spectroscopy (EIS) in an 80 mM borate buffer. First, we implemented bulk water electrolysis experiments over MnCl₂ and **1**. As shown in Fig. S31 red curve, after a short period of electrode activation ≈15 min, the current of MnCl₂ shows no evidence of the stability for the rest of the experiment over 3 h. After 3 h of electrolysis, the catalytic activity of the as-used electrode for repeating electrolysis experiment was checked in a buffer solution without MnCl₂ (Fig. S31 blue curve). The same catalytic current still keeps for the as-used one, which means manganese oxide resulted from Mn²⁺ (aq.) is the dominant active electrocatalyst. The deposited manganese oxide film was found on the surface of electrode and further was verified by electron microscopy (Fig. 8a,b). Bulk water electrolysis catalyzed by **1** was carried out under the same reaction conditions (Fig. 7 red curve). After a short period of electrode activation, the current remains constant for the rest of the experiment over 3 h. After 3 h of electrolysis, we checked the catalytic activity of the as-used electrode by repeating the electrolysis experiments in a buffer solution without **1**. The current decreased sharply and the value of it (Fig. 7 blue curve) is very close to the original one for the blank. It is worth noting that no deposited manganese oxide film was observed on the surface of electrode by eyesight. Meanwhile, in contrast with the bulk water electrolysis experiments over MnCl₂, the electrode surface of **1** looks clean with no sign of film deposition (Fig. 8c,d) confirmed by SEM and EDX analysis.

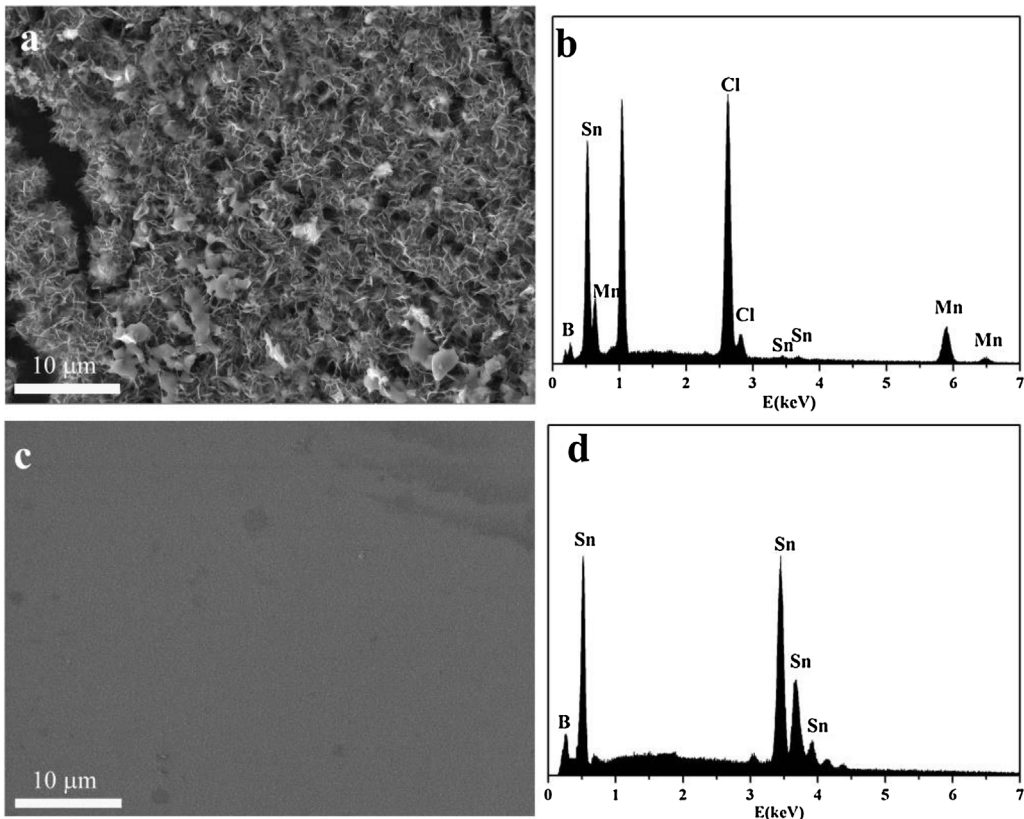


Fig. 8. Typical scanning electron microscopy (SEM) image and EDX histogram of the surface of a FTO glass electrode after 3 h of catalytic water electrolysis under an applied voltage of 1.2 V vs Ag/AgCl electrode in a pH = 9.0 sodium borate buffer (80 mM) solution, containing 0.5 mM MnCl₂ (a,b), 0.5 mM **1** (c,d).

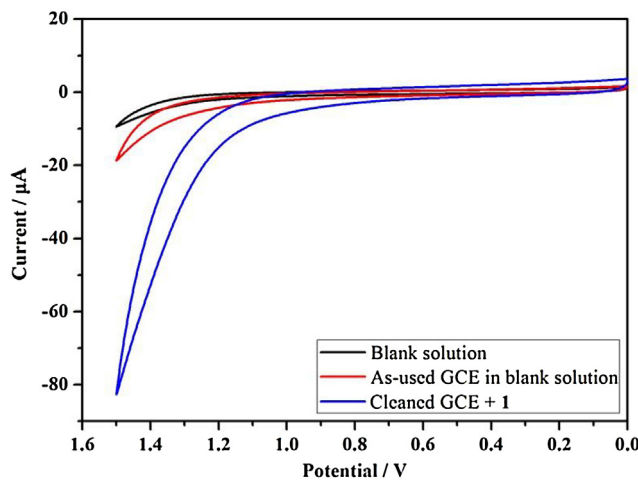


Fig. 9. CV curve of 0.5 mM **1** in 80 mM pH 9.0 borate buffer (blue curve) with cleaned glassy carbon electrode (GCE). Red curve shows the CV curve of the as-used GCE in 80 mM pH 9.0 borate buffer without **1**. Black curve shows the CV curve of cleaned GCE in 80 mM pH 9.0 borate buffer without **1** (i.e. blank solution). Conditions: glassy carbon working electrode, Ag/AgCl (saturate KCl) reference electrode and Pt wire counter electrode; scan rate 100 mV/s. (For interpretation of the references to colour in this figure legend, the reader is referred to the web version of this article.)

Second, the characterization of **1** by CV in borate buffer at pH 9.0 shows an intense onset anodic wave beginning at ca. 0.7 V (vs. Ag/AgCl electrode) and reaches a peak current of 85 μA (current density of 1.2 mA cm⁻²) at 1.5 V (Fig. 9). Then, the as-used electrode of the CV test on **1** was used for another CV test in the same buffered

solution without **1**. As depicted in Fig. 9, no evident catalytic current was detected with a value very close to the one for the original blank. As shown in Fig. S32, the CV of MnCl₂ shows two obvious oxidation peaks, while no oxidation peaks are observed for **1**. In order to explain the true active species in a further step, another group of CV tests were carried out. The as-used electrode of the CV test over MnCl₂ was used for another CV test in the same buffered solution without MnCl₂. The catalytic current shows nearly the same value as that test with the initial CV of MnCl₂, which means manganese oxide decomposed from MnCl₂ is the dominant active catalyst (Fig. S32 red curve). The results of all CV tests indicate that no other active species formed on the surface of electrode during the CV test procedure in the solution containing **1** and **1** is a homogeneous electrocatalytic WOC. This conclusion was further supported by the linear correlation experiment. A linear relationship between the catalytic current density of **1** at 1.5 V (vs. Ag/AgCl electrode) and the concentrations of **1** is observed, demonstrating **1** is stable and no MnO_x nanoparticles are formed during the electrocatalytic water oxidation process (Fig. 10).

Third, electrochemical impedance spectroscopy (EIS) can be used to differentiate the water oxidation behavior between polyoxometalate molecules and corresponding simple metal salts. Recently, we employed EIS method to confirm the differences in the electrochemical properties between polyoxometalate containing Ni and the equivalent Ni²⁺ (aq) for the first time [28]. The EIS tests were based on MnCl₂ and **1** by applying an AC voltage with 5 mV amplitude in a frequency ranging from 100 000 to 0.1 Hz in an 80 mM borate buffer solution (pH = 9.0). As shown in Fig. S33, comparing with the Mn²⁺ (aq.), **1** has a smaller semi-circular diameter. As a result, the charge transfer resistance of **1** and the Mn²⁺ (aq.) is completely different. Fourth, the current density of **1** as a function

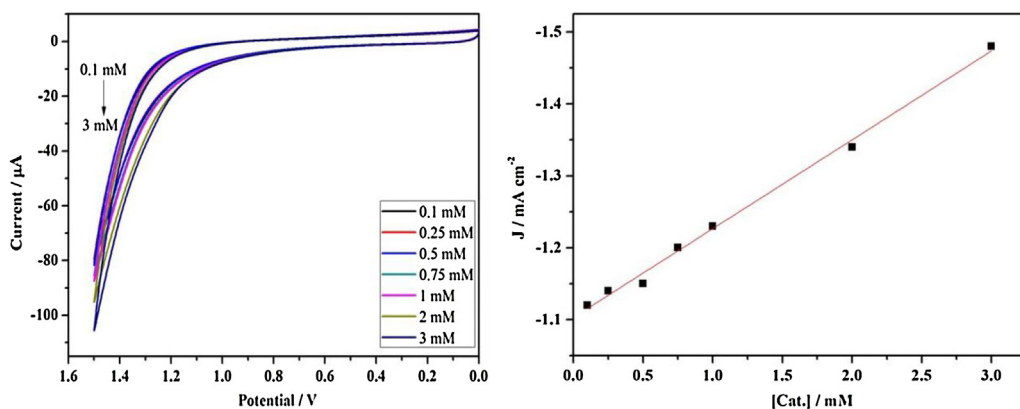


Fig. 10. (Left) CVs of different concentrations of **1** (0.1–3.0 mM) in 80 mM pH 9.0 borate buffer. Conditions: glassy carbon working electrode, Ag/AgCl (saturate KCl) reference electrode and Pt wire counter electrode; scan rate 100 mV/s. (Right) Plot of catalytic current density J at ~ 1.5 V vs Ag/AgCl electrode against the concentrations of **1**.

of the pH shows apparent distinction with that of the equivalent Mn^{2+} (aq.). The current density values of Mn^{2+} (aq.) show obvious changes with the variation of pHs (Fig. S34a, b). The catalytic current density of Mn^{2+} (aq.) increased greatly with the increase of pH. However, the catalytic current density of **1** shows little changes with the increase of pH (Fig. S34c, d). From the discussion above, we draw the conclusion that the electrocatalytic activity and electrocatalytic behavior between **1** and the equivalent Mn^{2+} (aq.) in water oxidation are completely different.

3.5. Effect of structure and catalytic activity

It can be concluded from the above experiments that the catalytic activities of **1–3** for water oxidation follow the order of **1 > 2 > 3**. As to the above three catalysts, structure and heteroatom are different, which lead to variation in charge, electron transport rate and different catalytic activity of water oxidation. The EIS and Tafel slopes were used to explore the reason for the different catalytic activities of **1–3** over water oxidation (Fig. S35 and S36). For charge-transfer resistance, the diameter of arc on EIS is a very important parameter and the value of diameter correlates with the charge and electron transfer reaction kinetics in the process of water oxidation [46]. According to Fig. S35, catalyst **1** possesses the smallest arc diameter and **3** has the largest one, which indicates that **1** has a small charge transfer resistance value and a fast electron and charge transfer rate. The above results of EIS indicate that **1** has higher electrocatalytic water oxidation activity than that of **2** and **3**, which can be confirmed further by the results of Tafel slope. As demonstrated in Fig. S36, the tafel slopes of **1–3** follow the order of **3 > 2 > 1**. The lowest tafel slope of **1** manifests that **1** has a fast electron and charge transfer rate, which is consistent with the EIS data.

In addition, to study the photocatalytic water oxidation ability of **1–3**, the band gap structures of the three catalysts were investigated. The band gap structures of **1–3** were verified by CVs and UV-vis diffuse reflectance spectra (Fig. S37, S38 and Table S3). The HOMO values of **1–3** are +1.31, +1.43 and +1.54 V, respectively. The potential difference ($\Delta E = \text{HOMO}([\text{Ru}(\text{bpy})_3]^{3+}) - \text{HOMO}(\text{catalyst})$) between $[\text{Ru}(\text{bpy})_3]^{3+}$ and catalysts increases with the order of $\Delta E(\text{3}) < \Delta E(\text{2}) < \Delta E(\text{1})$, indicating that the catalysts from **3**, **2** to **1** are more and more easily oxidized by $[\text{Ru}(\text{bpy})_3]^{3+}$. These data suggest that **1** has the highest charge transfer efficiencies between $[\text{Ru}(\text{bpy})_3]^{3+}$ and catalyst. Therefore, it is a relatively reasonable explanation that catalysts **1** has the best catalytic activity under both photocatalytic and electrocatalytic water oxidation conditions.

4. Conclusions

In summary, a series of different manganese-containing POMs were synthesized and characterized by multiple experiments. The catalytic water oxidation abilities of these catalysts were investigated in photochemical and electrochemical manner. A definite catalytic activity order of water oxidation is obtained: $[\text{Mn}_3(\text{H}_2\text{O})_3(\text{SbW}_9\text{O}_{33})_2]^{12-}$ (**1**) $> [\text{Mn}_3(\text{H}_2\text{O})_5(\text{PW}_9\text{O}_{34})_2]^{19-}$ (**2**) $> [\text{Mn}_3(\text{H}_2\text{O})_3(\text{AsW}_9\text{O}_{33})_2]^{12-}$ (**3**). The Mn_3 POM based on Sb heteroatom (**1**) has the best water oxidation activity under photochemical and electrochemical systems. The heteroatoms in the polyoxoanion play important role for the water oxidation activity. Among the known water oxidation catalysts based on POM containing Mn, for the first time, we implemented electrochemical impedance spectroscopy method to confirm the differences in the electrocatalytic water oxidation properties between POM containing Mn and the equivalent Mn^{2+} (aq.). Multiple experiments including UV-vis, IR, laser flash photolysis, THpANO₃ toluene extraction, capillary electrophoretic measurements and electrochemical experiments confirm that **1** is a homogeneous molecular catalyst rather than Mn^{2+} ions (aq) or manganese oxide during the water oxidation process.

Acknowledgements

This work was financially supported by the National Natural Science Foundation of China (Grant no. 21173105), Fundamental Research Funds for the Central Universities (Izujbky-2016-k08) and the Natural Science Foundation of Gansu (1506RJZA224).

Appendix A. Supplementary data

Supplementary data associated with this article can be found, in the online version, at <http://dx.doi.org/10.1016/j.apcatb.2017.02.061>.

References

- [1] M.W. Kanan, D.G. Nocera, *Science* 321 (2008) 1072–1075.
- [2] F. Jiao, H. Frei, *Energy Environ. Sci.* 3 (2010) 1018–1027.
- [3] X. Du, J. Zhao, J. Mi, Y. Ding, P. Zhou, B. Ma, J. Zhao, J. Song, *Nano Energy* 16 (2015) 247–255.
- [4] J.J. Stracke, R.G. Finke, *ACS Catal.* 4 (2014) 909–933.
- [5] B. Li, F. Li, S. Bai, Z. Wang, L. Sun, Q. Yang, C. Li, *Energy Environ. Sci.* 5 (2012) 8229–8233.
- [6] P.-E. Car, M. Guttentag, K.K. Baldridge, R. Alberto, G.R. Patzke, *Green Chem.* 14 (2012) 1680–1688.

- [7] M. Murakami, D. Hong, T. Suenobu, S. Yamaguchi, T. Ogura, S. Fukuzumi, *J. Am. Chem. Soc.* 133 (2011) 11605–11613.
- [8] S.M. Barnett, K.I. Goldberg, J.M. Mayer, *Nat. Chem.* 4 (2012) 498–502.
- [9] T. Zhang, C. Wang, S. Liu, J.L. Wang, W. Lin, *J. Am. Chem. Soc.* 136 (2014) 273–281.
- [10] G. Chen, L. Chen, S.M. Ng, T.C. Lau, *ChemSusChem* 7 (2014) 127–134.
- [11] M. Zhang, M. Zhang, C. Hou, Z. Ke, T. Lu, *Angew. Chem. Int. Ed.* 53 (2014) 13042–13048.
- [12] J.L. Fillol, Z. Codola, I. Garcia-Bosch, L. Gomez, J.J. Pla, M. Costas, *Nat. Chem.* 3 (2011) 807–813.
- [13] C. Panda, J. Debgupta, D. Diaz Diaz, K.K. Singh, S. Sen Gupta, B.B. Dhar, *Am. Chem. Soc.* 136 (2014) 12273–12282.
- [14] J. Soriano-Lopez, S. Goberna-Ferron, L. Vigara, J.J. Carbo, J.M. Poblet, J.R. Galan-Mascaros, *Inorg. Chem.* 52 (2013) 4753–4755.
- [15] F. Evangelisti, R. Guttinger, R. More, S. Luber, G.R. Patzke, *J. Am. Chem. Soc.* 135 (2013) 18734–18737.
- [16] R. Al-Oweini, A. Sartorel, B.S. Bassil, M. Natali, S. Berardi, F. Scandola, U. Kortz, M. Bonchio, *Angew. Chem. Int. Ed.* 53 (2014) 11182–11185.
- [17] L. Ma, Q. Wang, W.L. Man, H.K. Kwong, C.C. Ko, T.C. Lau, *Angew. Chem. Int. Ed.* 54 (2015) 5246–5249.
- [18] H. Dau, M. Haumann, *Coord. Chem. Rev.* 252 (2008) 273–295.
- [19] S.T. Zheng, G.Y. Yang, *Chem. Soc. Rev.* 41 (2012) 7623–7646.
- [20] F. Song, Y. Ding, C. Zhao, *Acta Chim. Sinica* 72 (2014) 133–144.
- [21] Y. Ji, L. Huang, J. Hu, C. Streb, Y. Song, *Energy Environ. Sci.* 8 (2015) 776–789.
- [22] S. Wang, G. Yang, *Chem. Rev.* 115 (2015) 4893–4962.
- [23] M. Ibrahim, A. Haider, Y. Lan, B.S. Bassil, A.M. Carey, R. Liu, G. Zhang, B. Keita, W. Li, G.E. Kostakis, A.K. Powell, U. Kortz, *Inorg. Chem.* 53 (2014) 5179–5188.
- [24] Z. Zhang, Q. Lin, S.T. Zheng, X. Bu, P. Feng, *Chem. Commun.* 47 (2011) 3918–3920.
- [25] L. Yu, X. Du, Y. Ding, H. Chen, P. Zhou, *Chem. Commun.* 51 (2015) 17443–17446.
- [26] G. Zhu, E.N. Glass, C. Zhao, H. Lv, J.W. Vickers, Y.V. Geletii, D.G. Musaev, J. Song, C.L. Hill, *Dalton Trans.* 41 (2012) 13043–13049.
- [27] X. Han, Y. Li, Z. Zhang, H. Tan, Y. Lu, E. Wang, *J. Am. Chem. Soc.* 137 (2015) 5486–5493.
- [28] L. Yu, Y. Ding, M. Zheng, H. Chen, J. Zhao, *Chem. Commun.* 52 (2016) 14494–14497.
- [29] X. Du, Y. Ding, F. Song, B. Ma, J. Zhao, J. Song, *Chem. Commun.* 51 (2015) 13925–13928.
- [30] Q. Yin, J.M. Tan, C. Besson, Y.V. Geletii, D.G. Musaev, A.E. Kuznetsov, Z. Luo, K.I. Hardcastle, C.L. Hill, *Science* 328 (2010) 342–345.
- [31] F. Song, Y. Ding, B. Ma, C. Wang, Q. Wang, X. Du, S. Fu, J. Song, *Energy Environ. Sci.* 6 (2013) 1170–1184.
- [32] W. Chen, X. Wang, C. Qin, K. Shao, Z. Su, E. Wang, *Chem. Commun.* 52 (2016) 9514–9517.
- [33] R. Xiang, Y. Ding, J. Zhao, *Chem. Asian J.* 9 (2014) 3228–3237.
- [34] H. Lv, J. Song, Y.V. Geletii, J.W. Vickers, J.M. Sumliner, D.G. Musaev, P. Kogerler, P.F. Zhuk, J. Bacsá, G. Zhu, C.L. Hill, *J. Am. Chem. Soc.* 136 (2014) 9268–9271.
- [35] J. Wei, Y. Feng, P. Zhou, Y. Liu, J. Xu, R. Xiang, Y. Ding, C. Zhao, L. Fan, C. Hu, *ChemSusChem* 8 (2015) 2630–2634.
- [36] X. Han, Z. Zhang, T. Zhang, Y. Li, W. Lin, W. You, Z. Su, E. Wang, *J. Am. Chem. Soc.* 136 (2014) 5359–5366.
- [37] Z. Huang, Z. Luo, Y.V. Geletii, J.W. Vickers, Q. Yin, D. Wu, Y. Hou, Y. Ding, J. Song, D.G. Musaev, C.L. Hill, T. Lian, *J. Am. Chem. Soc.* 133 (2011) 2068–2071.
- [38] B. Schwarz, J. Förster, M.K. Goetz, D. Yücel, C. Berger, T. Jacob, C. Streb, *Angew. Chem. Int. Ed.* 55 (2016) 6329–6333.
- [39] M.-P. Santoni, G. La Ganga, V. Mollica Nardo, M. Natali, F. Puntoriero, F. Scandola, S. Campagna, *J. Am. Chem. Soc.* 136 (2014) 8189–8192.
- [40] M. Bösing, A. Nöh, I. Loose, B. Krebs, *J. Am. Chem. Soc.* 120 (1998) 7252–7259.
- [41] M. Bösing, I. Loose, H. Pohlmann, B. Krebs, *Chem. Eur. J.* 3 (1997) 1232–1237.
- [42] P.J. Domaille, G. HervéA, A. TéazéA, Vanadium(V) substituted dodecatungstophosphates, in: *Inorg. Synth.*, John Wiley & Sons, Inc., 2007, 2017, pp. 96–104.
- [43] R. Al-Oweini, B.S. Bassil, T. Palden, B. Keita, Y. Lan, A.K. Powell, U. Kortz, *Polyhedron* 52 (2013) 461–466.
- [44] P. Mialane, J. Marrot, E. Rivière, J. Nebout, G. Hervé, *Inorg. Chem.* 40 (2001) 44–48.
- [45] H. Lv, Y.V. Geletii, C. Zhao, J.W. Vickers, G. Zhu, Z. Luo, J. Song, T. Lian, D.G. Musaev, C.L. Hill, *Chem. Soc. Rev.* 41 (2012) 7572–7589.
- [46] D. Guo, X. Qiu, W. Zhu, L. Chen, *Appl. Catal. B* 89 (2009) 597–601.